



# HHS Public Access

Author manuscript

*Biomacromolecules*. Author manuscript; available in PMC 2022 July 15.

Published in final edited form as:

*Biomacromolecules*. 2019 November 11; 20(11): 4208–4217. doi:10.1021/acs.biomac.9b01116.

## Differential Roles of Plasma Protein Corona on Immune Cell Association and Cytokine Secretion of Oligomeric and Fibrillar Beta-Amyloid

Ava Faridi<sup>†</sup>, Wen Yang<sup>‡</sup>, Hannah Gabrielle Kelly<sup>§,||</sup>, Chuanyu Wang<sup>‡</sup>, Pouya Faridi<sup>⊥</sup>, Anthony Wayne Purcell<sup>⊥</sup>, Thomas P. Davis<sup>\*,†,#</sup>, Pengyu Chen<sup>\*,‡</sup>, Stephen J. Kent<sup>\*,§,||,∇</sup>, Pu Chun Ke<sup>\*,†</sup>

<sup>†</sup>ARC Centre of Excellence in Convergent Bio-Nano Science and Technology, Monash Institute of Pharmaceutical Sciences, Monash University, 381 Royal Parade, Parkville, Victoria 3052, Australia

<sup>‡</sup>Materials Research and Education Center, Auburn University, Auburn, Alabama 36849, United States

<sup>§</sup>Department of Microbiology and Immunology, Peter Doherty Institute for Infection and Immunity, University of Melbourne, Melbourne, Victoria 3052, Australia

<sup>||</sup>ARC Centre for Excellence in Convergent Bio-Nano Science and Technology, University of Melbourne, Melbourne, Victoria 3052, Australia

<sup>⊥</sup>Infection and Immunity Program & Department of Biochemistry and Molecular Biology, Biomedicine Discovery Institute, Monash University, Clayton, Victoria 3800, Australia

<sup>#</sup>Australian Institute for Bioengineering and Nanotechnology, The University of Queensland, Brisbane, Queensland 4072, Australia

<sup>∇</sup>Melbourne Sexual Health Clinic and Infectious Diseases Department, Alfred Hospital, Monash University Central Clinical School, Carlton, Victoria 3053, Australia

### Abstract

Alzheimer's disease (AD) is a primary neurological disease with no effective cure. A hallmark of AD is the presence of intracellular tangles and extracellular plaques derived from the aberrant aggregation of tau- and beta-amyloid ( $A\beta$ ).  $A\beta$  presents in the brain as well as in cerebrospinal fluid and the circulation, and  $A\beta$  toxicity has been attributed to amyloidosis and inflammation, among other causes. In this study, the effects of the plasma protein corona have been investigated with regard to the blood cell association and cytokine secretion of oligomeric ( $A\beta_0$ ) and fibrillar

\*Corresponding Authors: thomas.p.davis@monash.edu, pengyuc@auburn.edu, skent@unimelb.edu.au, pu-chun.ke@monash.edu. Author Contributions

P.C.K. and P.C. designed the project. A.F. performed the TEM, ThT, and cell viability assays. S.J.K. and H.G.K. designed the blood assay. H.G.K. and A.F. performed the blood assay and data analysis. W.Y., C.W., and P.C. designed and performed the LSPR immunoassay and conducted data analysis. All authors provided feedback and agreed on the content of the manuscript.

#### Supporting Information

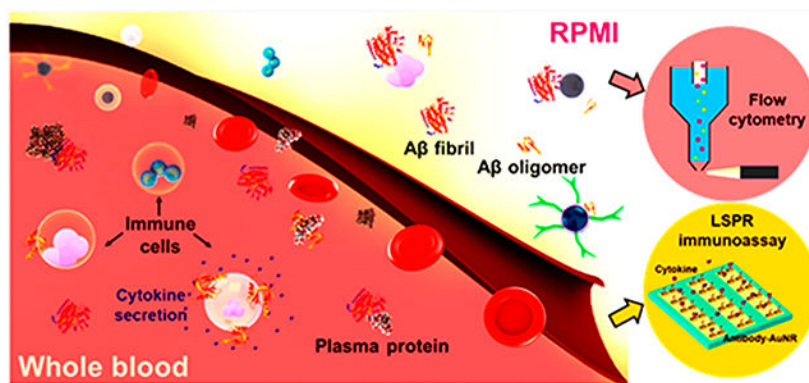
The Supporting Information is available free of charge on the [ACS Publications website](https://pubs.acs.org/doi/10.1021/acs.bio-mac.9b01116) at DOI: 10.1021/acs.bio-mac.9b01116.

Fabrication and measurement details of LSPR immunoassay; RP-HPLC elution of  $A\beta_m$ ,  $A\beta_0$ , and  $A\beta_f$  structures; and examples of gating related to cell association with ThT-labeled  $A\beta$  (PDF)

The authors declare no competing financial interest.

$A\beta_{1-42}$  ( $A\beta_f$ ), two major forms of the peptide aggregates.  $A\beta_o$  displayed little change in membrane association in whole blood or washed blood (i.e., cells in the absence of plasma proteins) at 37 °C, while  $A\beta_f$  showed a clear preference for binding with all cell types sans plasma proteins. Immune cells exposed to  $A\beta_o$ , but not to  $A\beta_f$ , resulted in significant expression of cytokines IL-6 and TNF measured in real-time by a localized surface plasmon resonance sensor. These observations indicate greater immune cell association and cytokine stimulation of  $A\beta_o$  than  $A\beta_f$  and shed new light on the contrasting toxicities of  $A\beta_o$  and  $A\beta_f$  resulting from their differential capacities in acquiring a plasma protein corona. These results further implicate a close connection between  $A\beta$  amyloidosis and immunopathology in AD.

## Graphical Abstract



## INTRODUCTION

Beta amyloid ( $A\beta$ ) originates from amyloid precursor protein (APP), an integral membrane protein expressed in tissues and especially in the brain. The APP is cleaved off by  $\beta$  and  $\gamma$  secretases, yielding two major peptide products  $A\beta_{1-40}$  and  $A\beta_{1-42}$ .<sup>1</sup> Among the two peptides,  $A\beta_{1-42}$  is more hydrophobic due to the two additional amino acids of isoleucine and alanine at the C-terminus and is considerably more cytotoxic due to its higher tendency in aberrant aggregation. The extracellular amyloid deposits of  $A\beta$  and the intracellular tangles of tau are two histopathological hallmarks of Alzheimer's disease (AD), a primary form of neurological disorder in aging populations.<sup>2</sup>

While  $A\beta$  plaques are often located in the brain tissues of AD patients postmortem, the peptide itself can also be traced in cerebrospinal fluid (CSF) and the circulation.<sup>3</sup> The relationship between the peptide levels in the brain, CSF, and plasma in healthy and diseased individuals, however, remains unclear.<sup>4</sup> Compelling evidence has shown the transport of  $A\beta$  by serum albumin and apolipoproteins in the blood plasma,<sup>5,6</sup> likely due to the poor solubility of the peptide as well as the chaperone-like capacity of serum albumin<sup>7-9</sup> against the conformational changes of  $A\beta$ . Furthermore, while specific receptors on microglia and monocytes/macrophages in the brain may determine the clearance of extracellular  $A\beta$  peptides through noninflammatory phagocytosis or pro-inflammatory cytokine secretion,<sup>10-14</sup> adherence of complement C3b to complement receptor 1 (CR1) of erythrocytes is a mechanism hypothesized for the peripheral clearance of  $A\beta$ .<sup>15</sup>

The literature has suggested the use of  $A\beta$  in the blood as an effective indicator for the early diagnosis of AD.<sup>16</sup> The effect of human serum albumin (HSA) on the reduction of  $\alpha$ -synuclein aggregation (associated with Parkinson's disease) has been reported recently.<sup>17</sup> However, the associations of plasma proteins and blood cells with  $A\beta$  in its major aggregation forms, namely, oligomers and amyloid fibrils (abbreviated as  $A\beta_O$  and  $A\beta_f$  hereafter, to refer to the chiefly oligomeric and fibrillar forms of the peptide), remain unclear. Furthermore, the immune responses of blood cells to amyloidogenic peptides and their aggregates have not been systematically investigated. To understand the transformation of  $A\beta$  in circulation, here we examined the binding of human blood cells with  $A\beta_O$  and  $A\beta_f$  with a special attention to plasma proteins, using a high-throughput blood association assay.<sup>18,19</sup> We further characterized real-time secretion of cytokines, i.e., interleukin 6 (IL-6) and tumor necrosis factor alpha (TNF), by human monocytes and lymphocytes exposed to  $A\beta_O$  and  $A\beta_f$ , using a localized surface plasmon resonance (LSPR) immunoassay.<sup>20</sup> Both our blood cell and LSPR immune assays implicated a significant role of plasma protein corona in shaping the cell binding affinity and toxicity of amyloid-protein aggregates and demonstrated a convoluted relationship between amyloidosis and inflammation in AD.

## MATERIALS AND METHODS

### $A\beta$ preparation.

Hexafluoro-2-propanol (HFIP)-treated human  $A\beta_{1-42}$  (AnaSpec, sequence, AIAEGDSHVLKEGAY-MEIFDVQGHVFGGKIFRVVDLGSNVA; purity, HPLC 95%; abbreviated as  $A\beta$  hereafter) was used in preparation of the two aggregating states of  $A\beta$ . Specifically,  $A\beta_O$  was rendered by incubating the freshly dissolved  $A\beta$  in 0.003%  $NH_4OH$  buffer at room temperature for 30 h, while  $A\beta_f$  was obtained by incubating the peptide at 37 °C for more than 60 h. The two aggregation states were confirmed by a ThT kinetic assay and TEM imaging.

### Transmission Electron Microscopy (TEM).

For TEM imaging, 5  $\mu L$  of  $A\beta_O$  and  $A\beta_f$  (each of 50  $\mu M$ ), plasma proteins,  $A\beta_O$ , and  $A\beta_f$  in interaction with plasma proteins were pipetted onto copper grids (400 mesh, glow-discharged for 15 s; Formvar film, ProSciTech) and let to adsorb for 1 min. After removing unbound samples by filter paper the grids were rinsed with 10  $\mu L$  of Milli-Q water. The grids were then negatively stained with 5  $\mu L$  of 1% uranyl acetate (UA) for 30 s and blown dry. The samples were imaged by a transmission electron microscope (Tecnai G2 F20, FEI, Eindhoven, The Netherlands) under an electric potential of 200 kV. Images were acquired with a CCD camera (UltraScan 1000, Gatan).

### Thioflavin T (ThT) Kinetic Assay.

A kinetic assay on peptide fibrillization was conducted using 50  $\mu M$   $A\beta$  and 100  $\mu M$  ThT dye pipetted into a 96-well plate (Costar). Changes in ThT fluorescence, indicating the  $\beta$ -sheet content in the sample, were recorded at 37 °C until the saturation phase after 60 h by a plate reader (PerkinElmer EnSight HH33400; Ex/Em, 440/485 nm). The assay was done with triplicate for each sample condition.

### Cell Culture and Toxicity Assay.

SH-SY5Y neuroblastoma cells were cultured in Dulbecco's modified Eagle's medium: Nutrient Mixture F-12 (DMEM/F12, ATCC) with 10% fetal bovine serum (FBS). For the viability assay, a 96-well plate (Costar) was pretreated with poly-L-lysine (Sigma, 0.01%), incubated at 37 °C (5% CO<sub>2</sub>) for 30 min, and washed with phosphate buffered saline (PBS) thrice. Approximately 60 000 cells were added to each well and incubated at 37 °C and 5% CO<sub>2</sub> to reach 80% confluency. Propidium iodide (PI, 1 μM) dye in fresh DMEM/F12 was added and incubated with the cells for 30 min. After optimization of concentrations, samples of 20 μM Aβ in the form of oligomers or fibrils were added to the wells. After 15 h of treatment, the cell viability was read by an Operetta instrument (PerkinElmer, 20× lens; numerical aperture, 0.7) at 37 °C with 5% CO<sub>2</sub>. The PI-positive apoptotic cells were counted by the mapping function of the instrument. Nine reads per well for samples of triplicate were acquired. Untreated cells were imaged as the control.

### Helium Ion Microscopy (HIM).

Whole and washed blood cells were treated with 10 μM Aβ<sub>O</sub> and Aβ<sub>f</sub> with and without plasma proteins. The samples were then treated by 2.5% paraformaldehyde and incubated at 4 °C for 10 h. After the incubation, the samples were centrifuged, and paraformaldehyde/medium was replaced every 2 h with gradient concentrations of ethanol (20%, 40%, 60%, 80%, and 95%). A 30 μL portion of each sample was transferred to a carbon tape and air-dried. The cell morphologies were visualized by Orion NanoFab (Zeiss).

### Association of Aβ Species with Human Immune Cells.

Fresh blood was drawn from a healthy donor into sodium heparin Vacuettes (Greiner Bio-One) in accordance with the University of Melbourne Human ethics approval 1443420 and the Australian National Health and Medical Research Council Statement on Ethical Conduct in Human Research. The blood cells were counted using a CELL-DYN Emerald analyzer (Abbott). To prepare washed blood cells, 10 mL of whole blood was topped up to 50 mL with PBS and spun down at 950g, for 10 min, with slow brake. The process was repeated four more times to collect washed blood cells. The removal of plasma proteins from the cells was indicated using a UV-vis spectrophotometer (Nanodrop 2000, Thermo Fisher), where the protein absorbance at 280 nm was absent to confirm their removal. The cells were resuspended in serum-free RPMI 1640 (Gibco) to keep the cell concentration of whole and washed blood consistent. ThT-labeled Aβ<sub>O</sub> or Aβ<sub>f</sub> was added to 100 μL of blood in triplicate at 5, 10, and 15 μM and incubated at 4 and 37 °C for 1 h. Pharm Lyse buffer (BD) was added to lyse red blood cells at 40× blood volume, followed by washing twice with 4 mL of PBS (500g, 7 min). The cells were phenotyped for 1 h on ice by titrating antibodies against CD3 AF700 (SP34-2, BD), CD14 APC-H7 (MΦP9, BD), CD56 PE (B159, BD), lineage-1 cocktail FITC (BD), HLA-DR PerCP-Cy5.5 (G46-6, BD), and CD19 BV650 (HIB19, Biolegend). Free antibodies were washed and removed by centrifugation (500g, 7 min) with a PBS buffer containing 0.5% w/v BSA and 2 mM EDTA at 4 °C. The cells were fixed by formaldehyde in PBS at 1% weight to volume ratio. The samples were analyzed for cell association using flow cytometry (LSRFortessa, BD Biosciences) and software FlowJo V10.

## LSPR Detection of Immune Cell Responses to A $\beta$ Species.

**Cell Culture.**—Jurkat human T cells (ATCC CRL-2901) were cultured in RPMI-1640 medium (ATCC) with 200  $\mu\text{g}/\text{mL}$  G428 and 10% FBS (ATCC). The cells were incubated at 37 °C with 5% CO<sub>2</sub> (Thermo Scientific). Epstein–Barr virus transformed human B lymphoblasts (ATCC) were cultured in RPMI-1640 medium with 10% FBS. Human monocytic THP-1 cells (ATCC) were cultured in RPMI-1640 medium with 50  $\mu\text{M}$  mercaptoethanol and 10% FBS. The cell culture was maintained by replenishing the medium every 2–3 days at  $1 \times 10^5$  to  $1 \times 10^6$  cells/mL. The cells were collected by centrifugation (125g, 5 min) and resuspended in fresh culture medium.

**LSPR Immunoassay.**—The human immune cell lines (T cells, B cells, or THP-1 cells) were resuspended in human plasma proteins (Innovative Research) and RPMI-1640 medium at  $1 \times 10^6$  cells/mL, respectively. The immune cells were incubated with A $\beta_0$  and A $\beta_f$  of 5, 10, and 15  $\mu\text{M}$  final concentrations for 2 h at 4 and 37 °C. The immune responses of human THP-1 cells, human Jurkat T cells, and human B cells were investigated after stimulations with A $\beta_0$  and A $\beta_f$ . After 2 h of incubation, the culture medium was extracted and pipetted into an LSPR immunoassay chip (for fabrication and measurement details, see the description in the Supporting Information, as well as Figure S1) for the detection of secretory cytokines from the immune cells. A total of more than 100 chips were used for this assay.

## RESULTS AND DISCUSSION

### Interactions of A $\beta$ Aggregates with Plasma Proteins.

Due to the kinetic nature of amyloidosis, which is a convolution of both primary and secondary nucleation followed by elongation and saturation,<sup>1</sup> the A $\beta_0$  and A $\beta_f$  samples were not pure oligomers or fibrils but were inclusive of a collection of minor heterogeneous aggregates. Indeed, the reverse phase HPLC (RP-HPLC; for the method, see the Supporting Information) revealed formation of slightly hydrophobic A $\beta_0$  from its hydrophilic monomeric origin (centered on the retention time of ~20 min). As for the A $\beta_f$  sample, the monomeric and oligomeric species were depleted and converted into fibrillar structures of varying hydrophobicity (Figure S2).

The interaction of A $\beta$  with blood components is of intense interest as it offers a model to understand the immune response to amyloid proteins. Previously, Kuo et al. reported the interactions of fresh A $\beta_{1-40}$  and A $\beta_{1-42}$  with plasma proteins.<sup>21</sup> Here, our TEM imaging of plasma proteins, and A $\beta_0$  and A $\beta_f$  with and without plasma proteins confirmed the two aggregation states as globules and fibrils (Figure 1a,b), respectively. TEM imaging showed the morphologies of plasma proteins (Figure 1c) and their associations with the A $\beta$  species (Figure 1d,e). Specifically, in the case of A $\beta_f$ , a protein “corona” was rendered upon the peptide incubation with plasma proteins, mediated by H-bonding and electrostatic interactions between the A $\beta_f$  surface moieties and the amphiphilic plasma proteins.<sup>22</sup>

### **A $\beta$ Aggregation Kinetics and Cytotoxicity.**

The ThT kinetics of A $\beta$ <sub>m</sub> and A $\beta$ <sub>O</sub> displayed a nucleation phase, followed by an elongation phase to a saturation phase of the peptide after ~60 h (Figure 1f). This result is consistent with the A $\beta$  fibrillization in the literature.<sup>23–25</sup> In the presence of plasma proteins, interactions of both A $\beta$ <sub>m</sub> and A $\beta$ <sub>O</sub> with the proteins blocked the addition of A $\beta$  monomers to inhibit the further assembly of the oligomers into amyloid fibrils.

Aggregation of amyloid proteins is a hallmark of neuro-degenerative diseases and type 2 diabetes. A $\beta$  aggregation is associated with neuronal cell degeneration,<sup>26–28</sup> and the A $\beta$  oligomers are considered to be the most toxic species.<sup>29,30</sup> The cytotoxicity of A $\beta$  in this study was consistent with the literature and with the aggregation inhibition of A $\beta$  in interaction with plasma proteins (Figure 2a), revealing suppressed toxicity of A $\beta$ <sub>O</sub> with plasma proteins ( $39 \pm 2.6\%$  without plasma proteins down to  $30 \pm 2\%$  with plasma proteins). In comparison, A $\beta$ <sub>f</sub> induced a modest 13% cytotoxicity which was not affected by plasma proteins.

### **A $\beta$ Aggregation-Induced Membrane Damage.**

The morphologies of SH-SY5Y neuronal cells exposed to the two A $\beta$  aggregating species were examined with helium ion microscopy (HIM). HIM utilizes a helium ion source to excite a small sample volume with a large depth and is advantageous to conventional scanning electron microscopy in both resolution and image brightness. Consistent with the viability assay, significant damage including membrane deformation and blebbing of the SH-SY5Y cells was observed upon their exposure to A $\beta$ <sub>O</sub> (Figure 2b), while such damage was reduced in the presence of A $\beta$ <sub>O</sub> incubated with plasma proteins. In comparison, no damage was evident when the cells were exposed to A $\beta$ <sub>f</sub> with or without plasma proteins.

### **Cell Associations with A $\beta$ Aggregates.**

In recent research, AD is considered as more than a neural-centric disease but has its origin in the immune system and inflammation.<sup>31,32</sup> To better understand the interaction between A $\beta$  and blood immune cells, the association of fresh human blood phagocytes (granulocytes, monocytes, and dendritic cells) and lymphocytes (T cells, B cells, and natural killer/NK cells) with A $\beta$ <sub>O</sub> and A $\beta$ <sub>f</sub> in the presence and absence of plasma proteins was assessed by flow cytometry (Figures 3 and 4). The A $\beta$  structures displayed no apparent association with any type of the immune cells at 4 °C in either whole blood or washed blood. An increment of temperature from 4 to 37 °C, which elevated biomolecular diffusion as well as the biological processes of endocytosis and phagocytosis uptake,<sup>19</sup> gave rise to increased association of A $\beta$  with all types of the immune cells. Although the most prominent association of the A $\beta$  proteins was with blood immune cells of phagocytic nature (granulocytes, monocytes, and dendritic cells), substantial association was also observed for B and T lymphocytes (Figure 4).

The amphiphilic structures of oligomers and protofibrils, known as the most toxic species of A $\beta$ ,<sup>1</sup> are less prone to interact with the hydrophilic surfaces of plasma proteins and biomolecules. On the other hand, amyloid peptides and proteins show a high propensity for cell membranes by initiating contact via the N termini of their functional monomers,



which triggers their structural transition from monomers to alpha helices, toxic oligomers, and protofibrils, and, eventually,  $\beta$ -sheet rich amyloid fibrils.<sup>1</sup> Consistent with these known biochemical properties, we found that  $A\beta_0$  displayed strong and comparable associations with the neuronal cells in both whole blood and washed blood cells (i.e., with plasma proteins removed, Figure 4). In contrast,  $A\beta_f$  showed less association with the immune cells compared to  $A\beta_0$ . We hypothesized that this is likely due to the high capacity of  $A\beta_f$  to establish hydrogen bonds with free plasma proteins, forming a nonspecific protein corona around the  $A\beta_f$  when incubated with whole blood.<sup>33</sup> Indeed, we observed that  $A\beta_f$  association with immune cells in whole blood (with plasma proteins) was generally greater than that observed in washed blood (without plasma proteins). This was particularly evident in the lymphocyte population (T, B, NK cells) where association was almost completely abrogated, with a less marked effect on granulocytes and dendritic cells.

The association of  $A\beta$  aggregates with plasma proteins entails both physical and toxicological implications. Serum albumin, the most abundant protein in the plasma, has been shown to inhibit  $A\beta_{1-40}$  aggregation.<sup>34,35</sup> The higher level of toxic  $A\beta$  association with cell membranes can result in an elevated response from monocytes among immune cells.<sup>34</sup> Previous studies showed that the accumulations of  $A\beta$ , microglia, as well as blood monocyte macrophages were significantly involved in anti-inflammatory response to excess  $A\beta$ .<sup>36,37</sup> In this study, we noted a high level of interaction between the  $A\beta$  species and monocytes for all conditions (i.e., 90–100% for all concentrations of  $A\beta_0$  and 20–40% and 60–80% for low and high concentrations of  $A\beta_f$ , respectively; Figure 4). Overall, the monocytes displayed the highest association with  $A\beta_0$  compared to other types of blood cells.

In addition to monocytes, recruitment of T cells at  $A\beta$  plaques has been reported.<sup>38</sup> T cells play a major role in the pathophysiology of AD,<sup>39</sup> where the cellular response induced a near complete clearance of  $A\beta$ .<sup>38</sup> In addition, research has shown that AD patients exhibit an elevated T cell response to  $A\beta$  as compared to middle-aged healthy individuals.<sup>40</sup> The telomere length of T cells is dysregulated in AD patients, which may have consequential effects on the immune system and the brain.<sup>41</sup> In the present study, strong associations of  $A\beta_0$  (i.e., 37–41%, 55–60%, and 66–67% for the three chosen concentrations) with T cells, independent of the presence of plasma proteins, were observed. In comparison,  $A\beta_f$  showed lower interactions with the T cells ( $5.2 \pm 0.1\%$ ,  $38.2 \pm 3.2\%$ , and  $51.8 \pm 1.5\%$  for the three chosen concentrations) without plasma proteins, and no significant interactions (<10%) with plasma proteins (Figure 4).

Dendritic cells (DCs), an initiator of adaptive immune responses, were reported to endocytose amyloid fibrils.<sup>14</sup> While the age-related behavior of DCs in enhancing peripheral inflammation has been documented, no significant changes in the secretion of chemokines or cytokines have been recorded with  $A\beta$  fibrils.<sup>42</sup> Here, association of 78–85% of  $A\beta_0$  in the absence of plasma proteins and stronger association of 69–93% of  $A\beta_0$  with DCs were recorded in whole blood cells.  $A\beta_f$ , in contrast, showed weaker interactions with DCs than  $A\beta_0$  at  $11.1 \pm 3.7\%$ ,  $35 \pm 0.7\%$ , and  $56.5 \pm 13\%$  and  $38.2 \pm 3.3\%$ ,  $69.2 \pm 3.1\%$ , and  $71.2 \pm 6.4\%$  for the three concentrations with and without plasma proteins, respectively (Figure 4).

Previous studies revealed hindered circulation of low-density granulocytes in AD-type dementia patients, suggesting a damaging effect of AD on inflammatory cells in the periphery.<sup>43</sup> In the current study, a strong association of  $A\beta_O$  with granulocytes (80–90%) was recorded with no considerable difference with and without plasma proteins. In the case of  $A\beta_f$ , the associations were determined to be  $7.0 \pm 2.9\%$ ,  $21.6 \pm 1.2\%$ , and  $35.7 \pm 2.6\%$  and  $11.7 \pm 0.4\%$ ,  $38.5 \pm 5.4\%$ , and  $51.8 \pm 3.1\%$  with and without plasma proteins, respectively (Figure 4). In addition to the blood cells characterized, a very low association of NK cells with  $A\beta_O$  and no association with  $A\beta_f$ , especially with plasma proteins, were observed.

The production of antibodies by B cells toward  $A\beta_{42}$  protofibrils has been shown to be much enhanced in AD patients as compared to healthy individuals.<sup>44</sup> In the present study, both  $A\beta$  species displayed interactions with B cells. Specifically, association of  $A\beta_O$  with B cells slightly decreased from whole blood to washed cells for the 3 concentrations of  $A\beta_O$  and significantly dropped from  $12.8 \pm 5.9\%$ ,  $36.6 \pm 6.0\%$ , and  $57.1 \pm 0.9\%$  to below 5% for the 3 concentrations of  $A\beta_f$ , respectively (Figure 4).

### **$A\beta_O$ - and $A\beta_f$ -Induced Immune Responses with and without Plasma Proteins.**

The deposition of  $A\beta$  peptide has been revealed to trigger a range of inflammation responses from immune cells to express cytokines and chemokines.<sup>45</sup> Laboratory and clinical investigations have shown evidence of increased release of pro-inflammatory cytokines in both the brain and plasma of AD patients.<sup>46</sup> In addition, plasma proteins including HSA have been demonstrated to mitigate  $A\beta$  amyloidosis and participate in AD-incited inflammatory responses in the brain. HSA binds 90% of plasma  $A\beta$  and could potentially affect their molecular distribution and pharmacokinetics.<sup>47</sup> Unveiling the influence of plasma proteins on the  $A\beta$  peptide-induced immune response and understanding the pro-inflammatory cytokine release profiles upon stimulation may offer new insights into  $A\beta$ -induced cytotoxicity to facilitate the development of AD therapy. Conventional cytokine detection methods such as enzyme-linked immunosorbent assay (ELISA) usually require laborious reagent processing procedures, including multiple steps of staining, washing, and blocking, and posing challenges in real-time analysis of dynamic molecular release processes.<sup>20</sup> In this study, we performed a label-free microfluidic-based LSPR immunoassay for real-time detection of multiple cytokines secreted by three types of immune cells, after coculturing the cells with  $A\beta_O$  or  $A\beta_f$ . The immune responses induced by  $A\beta_O$  and  $A\beta_f$  with and without plasma proteins were assessed by the levels of cytokine secretion.

Immune cell lines (T cells, B cells, or monocytic cells) were incubated with the two types of  $A\beta$  aggregates in human plasma and RPMI medium at 4 and 37 °C, respectively. LSPR immunoassay chips consisting of antibody-functionalized gold nanorods (AuNRs) were used to detect TNF and IL-6 secreted by the immune cells (Figure 5a). Cytokine binding with AuNR–antibody conjugate altered the localized-refractive index and enlarged the scattering cross section of the nanostructure. The plasmon resonance gave rise to a red shift in the scattering spectrum, coupled with an increased scattering intensity (Figure 5b). Images of the sensing spot arrays were acquired in real-time by an ultrasensitive electron multiplying CCD (EMCCD, Photometrics). The scattering intensities of the sensing



spots were processed by MATLAB and converted to cytokine concentrations based on pre-established calibrations (Figure 5c). More pronounced inflammatory responses were observed for immune cells exposed to the  $A\beta$  species at 37 °C than at 4 °C due to higher cell activity and metabolism (Figure 6). Specifically,  $A\beta_O$  induced overall heightened immune responses as compared to  $A\beta_f$  at 37 °C, suggesting stronger interaction and toxicity of the former with the immune cells. THP-1 cells (as a model system for monocytes), in particular, displayed a prominent pro-inflammatory cytokine secretion upon exposure to  $A\beta_O$ , consistent with the observed monocyte association with the  $A\beta$  aggregate (Figure 4).

Contrasting effects of plasma proteins on  $A\beta_O$ - and  $A\beta_f$ -induced immune responses were observed at 37 °C. Whereas  $A\beta_f$  displayed overall suppressed immune responses after interacting with plasma proteins for all three types of immune cells,  $A\beta_O$ -associated immune toxicity was mostly promoted in the presence of plasma proteins, except for TNF expression from the THP-1 cells. Such differential immune toxicity of  $A\beta$  depositions can be attributed to two main factors: size and hydrophobicity, correlating to the capacities of the  $A\beta$  species and their protein-coronae to bind and penetrate the immune cell membranes. It was reported that amylin oligomers of smaller size and higher hydrophobicity elicited a stronger immune response than their counterparts with similar size but less solvent-exposed hydrophobic residues.<sup>48,49</sup> As such, binding of  $A\beta_O$  with serum albumin in plasma proteins inhibited the peptide aggregation to maintain their small size and surface hydrophobicity, facilitating immune cell interactions to elevate immune responses.<sup>35</sup> In contrast,  $A\beta_f$  with lower structural plasticity and less exposed hydrophobic residues tends to bind to plasma proteins via charged and polar groups, resulting in a larger colloidal-like amyloid-protein corona while displaying weaker toxicity. It should be noted that TNF expression from THP-1 cells could be promoted through receptor-specific signaling pathways such as the Mac-1 receptor.<sup>50</sup> Hence, the formation of an  $A\beta_O$ -plasma protein corona could potentially shield the exposed  $A\beta_O$  activation motifs and drastically prohibit TNF secretion. Such a phenomenon was not observed for Mac-1 receptor-negative T-cells and B-cells.

## CONCLUSION

Amyloidosis has been extensively investigated for the past decades, driven by the urgent need to find a cure for amyloid diseases.<sup>1</sup> Much of this research emphasis has been centered on the amyloid hypothesis<sup>51</sup> and its pathological implications. The oligomers are widely viewed as the most toxic products of protein aggregation as established by extensive *in vitro* and *in vivo* data,<sup>52,53</sup> while amyloid fibrils are generally considered as benign despite experimental discrepancies.<sup>54</sup> Here, we have revealed a convoluted relationship between the amyloidosis and immunogenicity of  $A\beta_{1-42}$ , using a high-throughput blood assay and a label-free microfluidic-based LSPR immunoassay. Specifically,  $A\beta_O$  displayed strong blood cell association independent of plasma proteins. In contrast, binding of  $A\beta_f$  with the cells was weaker and was further dampened in whole blood as a result of a protein corona. Consistently, the LSPR immunoassay revealed elevated cytokine secretion of immune cells against both  $A\beta_O$  and  $A\beta_f$ , especially more so for the oligomers. The  $A\beta_f$ -elicited immune response was screened by plasma proteins, via a protein corona mediated by nonspecific forces. The oligomers, on the other hand, maintained their capacity for immune cell association due to their small size and finite hydrophobicity. This study has implicated the

intertwined relationship between the amyloidosis and immunogenicity of A $\beta$ , two aspects underlining the pathological cascade and therapeutic solution of AD.

## Supplementary Material

Refer to Web version on PubMed Central for supplementary material.

## ACKNOWLEDGMENTS

This work was supported by ARC Grant CE140100036 (T.P.D.), the National Science Foundation Grant CBET-1701363 (P.C.), the National Institutes of Health Grant R35GM133795 (P.C.), and AFTAM Research Collaboration Award (T.P.D. and P.C.K.). HIM imaging was performed by Anders Barlow at the MCFP platform, University of Melbourne.

## REFERENCES

- (1). Ke PC; Sani MA; Ding F; Kakinen A; Javed I; Separovic F; Davis TP; Mezzenga R Implications of Peptide Assemblies in Amyloid Diseases. *Chem. Soc. Rev* 2017, 46, 6492–6531. [PubMed: 28702523]
- (2). Ballard C; Gauthier S; Corbett A; Brayne C; Aarsland D; Jones E Alzheimer's Disease. *Lancet* 2011, 377, 1019–1031. [PubMed: 21371747]
- (3). Tublin JM; Adelstein JM; Del Monte F; Combs CK; Wold LE Getting to the Heart of Alzheimer Disease. *Circ. Res* 2019, 124, 142–149. [PubMed: 30605407]
- (4). Mackic JB; Bading J; Ghiso J; Walker L; Wisniewski T; Frangione B; Zlokovic BV Circulating Amyloid-Beta Peptide Crosses the Blood-Brain Barrier in Aged Monkeys and Contributes to Alzheimer's Disease Lesions. *Vasc. Pharmacol* 2002, 38, 303–313.
- (5). Biere AL; Ostaszewski B; Stimson ER; Hyman BT; Maggio JE; Selkoe DJ Amyloid Beta-Peptide is Transported on Lipoproteins and Albumin in Human Plasma. *J. Biol. Chem* 1996, 271, 32916–32922. [PubMed: 8955133]
- (6). Matsubara E; Sekijima Y; Tokuda T; Urakami K; Amari M; Shizuka-Ikeda M; Tomidokoro Y; Ikeda M; Kawarabayashi T; Harigaya Y; Ikeda S; Murakami T; Abe K; Otomo E; Hirai S; Frangione B; Ghiso J; Shoji M Soluble Abeta Homeostasis in AD and DS: Impairment of Anti-Amyloidogenic Protection by Lipoproteins. *Neurobiol. Aging* 2004, 25, 833–841. [PubMed: 15212837]
- (7). Finn TE; Nunez AC; Sunde M; Easterbrook-Smith SB Serum Albumin Prevents Protein Aggregation and Amyloid Formation and Retains Chaperone-like Activity in the Presence of Physiological Ligands. *J. Biol. Chem* 2012, 287, 21530–21540. [PubMed: 22549788]
- (8). Algamil M; Milojevic J; Jafari N; Zhang W; Melacini G Mapping the Interactions between the Alzheimer's Abeta-peptide and Human Serum Albumin beyond Domain Resolution. *Biophys. J* 2013, 105, 1700–1709. [PubMed: 24094411]
- (9). Kakinen A; Javed I; Faridi A; Davis TP; Ke PC Serum Albumin Impedes the Amyloid Aggregation and Hemolysis of Human Islet Amyloid Polypeptide and Alpha Synuclein. *Biochim. Biophys. Acta, Biomembr* 2018, 1860, 1803–1809. [PubMed: 29366673]
- (10). Ramanathan A; Nelson AR; Sagare AP; Zlokovic BV Impaired Vascular-Mediated Clearance of Brain Amyloid Beta in Alzheimer's Disease: the Role, Regulation and Restoration of LRP1. *Front. Aging Neurosci* 2015, 7, 136. [PubMed: 26236233]
- (11). Marsh SE; Abud EM; Lakatos A; Karimzadeh A; Yeung ST; Davtyan H; Fote GM; Lau L; Weinger JG; Lane TE; Inlay MA; Poon WW; Blurton-Jones M The Adaptive Immune System Restrains Alzheimer's Disease Pathogenesis by Modulating Microglial Function. *Proc. Natl. Acad. Sci. U. S. A* 2016, 113, E1316–E1325. [PubMed: 26884167]
- (12). Rogers J; Strohmeyer R; Kovelowski CJ; Li R Microglia and Inflammatory Mechanisms in the Clearance of Amyloid Beta Peptide. *Glia* 2002, 40, 260–269. [PubMed: 12379913]
- (13). Wang ZT; Zhong XL; Tan MS; Wang HF; Tan CC; Zhang W; Zheng ZJ; Kong LL; Tan L; Sun L Association of Lectin-like Oxidized Low Density Lipoprotein Receptor 1 (OLR1)

- Polymorphisms with Late-Onset Alzheimer Disease in Han Chinese. *Ann. Transl. Med* 2018, 6, 172. [PubMed: 29951494]
- (14). Marx F; Blasko I; Pavelka M; Grubeck-Loebenstien B The Possible Role of the Immune System in Alzheimer's Disease. *Exp. Gerontol* 1998, 33, 871–881. [PubMed: 9951630]
- (15). Rogers J; Li R; Mastroeni D; Grover A; Leonard B; Ahern G; Cao P; Kolody H; Vedders L; Kolb WP; Sabbagh M Peripheral Clearance of Amyloid Beta Peptide by Complement C3-Dependent Adherence to Erythrocytes. *Neurobiol. Aging* 2006, 27, 1733–1739. [PubMed: 16290270]
- (16). Pesini P; Perez-Grijalba V; Monleon I; Boada M; Tarraga L; Martinez-Lage P; San-Jose I; Sarasa M Reliable Measurements of the Beta-Amyloid Pool in Blood Could Help in the Early Diagnosis of AD. *Int. J. Alzheimer's Dis* 2012, 2012, 604141. [PubMed: 22957297]
- (17). Bellomo G; Bologna S; Cerofolini L; Paciotti S; Gatticchi L; Ravera E; Parnetti L; Fragai M; Luchinat C Dissecting the Interactions between Human Serum Albumin and  $\alpha$ -Synuclein: New Insights on the Factors Influencing  $\alpha$ -Synuclein Aggregation in Biological Fluids. *J. Phys. Chem. B* 2019, 123, 4380–4386. [PubMed: 31034772]
- (18). Weiss ACG; Kelly HG; Faria M; Besford QA; Wheatley AK; Ang CS; Crampin EJ; Caruso F; Kent SJ Link between Low-Fouling and Stealth: A Whole Blood Biomolecular Corona and Cellular Association Analysis on Nanoengineered Particles. *ACS Nano* 2019, 13, 4980–4991. [PubMed: 30998312]
- (19). Glass JJ; Chen L; Alcantara S; Crampin EJ; Thurecht KJ; De Rose R; Kent SJ Charge Has a Marked Influence on Hyperbranched Polymer Nanoparticle Association in Whole Human Blood. *ACS Macro Lett.* 2017, 6, 586–592. [PubMed: 35650842]
- (20). Javed I; He J; Kakinen A; Faridi A; Yang W; Davis TP; Ke PC; Chen P Probing the Aggregation and Immune Response of Human Islet Amyloid Polypeptides with Ligand-Stabilized Gold Nanoparticles. *ACS Appl. Mater. Interfaces* 2019, 11, 10462–10471. [PubMed: 30663303]
- (21). Kuo YM; Kokjohn TA; Kalback W; Luehrs D; Galasko DR; Chevallier N; Koo EH; Emmerling MR; Roher AE Amyloid-Beta Peptides Interact with Plasma Proteins and Erythrocytes: Implications for Their Quantitation in Plasma. *Biochem. Biophys. Res. Commun* 2000, 268, 750–756. [PubMed: 10679277]
- (22). Pilkington EH; Gustafsson OJR; Xing Y; Hernandez-Fernaund J; Zampronio C; Kakinen A; Faridi A; Ding F; Wilson P; Ke PC; Davis TP Profiling the Serum Protein Corona of Fibrillar Human Islet Amyloid Polypeptide. *ACS Nano* 2018, 12, 6066–6078. [PubMed: 29746093]
- (23). Sudhakar S; Kalipillai P; Santhosh PB; Mani E Role of Surface Charge of Inhibitors on Amyloid Beta Fibrillation. *J. Phys. Chem. C* 2017, 121, 6339–6348.
- (24). Knowles TP; Vendruscolo M; Dobson CM The Amyloid State and Its Association with Protein Misfolding Diseases. *Nat. Rev. Mol. Cell Biol* 2014, 15, 384–396. [PubMed: 24854788]
- (25). Shozawa H; Oguchi T; Tsuji M; Yano S; Kiuchi Y; Ono K Supratherapeutic Concentrations of Cilostazol Inhibits Beta-Amyloid Oligomerization in Vitro. *Neurosci. Lett* 2018, 677, 19–25. [PubMed: 29684530]
- (26). Wiltzius JJ; Sievers SA; Sawaya MR; Eisenberg D Atomic structures of IAPP (amylin) Fusions Suggest a Mechanism for Fibrillation and the Role of Insulin in the Process. *Protein Sci.* 2009, 18, 1521–1530. [PubMed: 19475663]
- (27). Zhang X; St. Clair JR; London E; Raleigh DP Islet Amyloid Polypeptide Membrane Interactions: Effects of Membrane Composition. *Biochemistry* 2017, 56, 376–390. [PubMed: 28054763]
- (28). Pilkington EH; Lai M; Ge X; Stanley WJ; Wang B; Wang M; Kakinen A; Sani MA; Whittaker MR; Gurzov EN; Ding F; Quinn JF; Davis TP; Ke PC Star Polymers Reduce Islet Amyloid Polypeptide Toxicity via Accelerated Amyloid Aggregation. *Biomacromolecules* 2017, 18, 4249–4260. [PubMed: 29035554]
- (29). Haataja L; Gurlo T; Huang CJ; Butler PC Islet Amyloid in Type 2 Diabetes, and the Toxic Oligomer Hypothesis. *Endocr. Rev* 2008, 29, 303–316. [PubMed: 18314421]
- (30). Faridi A; Sun Y; Okazaki Y; Peng G; Gao J; Kakinen A; Faridi P; Zhao M; Javed I; Purcell AW; Davis TP; Lin S; Oda R; Ding F; Ke PC Mitigating Human IAPP Amyloidogenesis In Vivo with Chiral Silica Nanoribbons. *Small* 2018, 14, No. 1802825.
- (31). Cao W; Zheng H Peripheral Immune System in Aging and Alzheimer's Disease. *Mol. Neurodegener* 2018, 13, 51. [PubMed: 30285785]

- (32). Solana C; Tarazona R; Solana R Immunosenescence of Natural Killer Cells, Inflammation, and Alzheimer's Disease. *Int. J. Alzheimer's Dis* 2018, 2018, 3128758. [PubMed: 30515321]
- (33). Cedervall T; Lynch I; Lindman S; Berggård T; Thulin E; Nilsson H; Dawson KA; Linse S Understanding the Nano-particle-Protein Corona Using Methods to Quantify Exchange Rates and Affinities of Proteins for Nanoparticles. *Proc. Natl. Acad. Sci. U. S.A* 2007, 104, 2050–2055. [PubMed: 17267609]
- (34). Reyes Barcelo AA; Gonzalez-Velasquez FJ; Moss MA Soluble Aggregates of the Amyloid-Beta Peptide are Trapped by Serum Albumin to Enhance Amyloid-Beta Activation of Endothelial Cells. *J. Biol. Eng* 2009, 3, 5. [PubMed: 19397812]
- (35). Milojevic J; Esposito V; Das R; Melacini G Understanding the Molecular Basis for the Inhibition of the Alzheimer's A $\beta$ -Peptide Oligomerization by Human Serum Albumin Using Saturation Transfer Difference and Off-resonance Relaxation NMR Spectroscopy. *J. Am. Chem. Soc* 2007, 129, 4282–4290. [PubMed: 17367135]
- (36). Wang MM; Miao D; Cao XP; Tan L; Tan L Innate Immune Activation in Alzheimer's Disease. *Ann. Trans. Med* 2018, 6, 177.
- (37). Michaud JP; Bellavance MA; Prefontaine P; Rivest S Real-Time in Vivo Imaging Reveals the Ability of Monocytes to Clear Vascular Amyloid Beta. *Cell Rep* 2013, 5, 646–653. [PubMed: 24210819]
- (38). Fisher Y; Nemirovsky A; Baron R; Monsonego A T Cells Specifically Targeted to Amyloid Plaques Enhance Plaque Clearance in a Mouse Model of Alzheimer's Disease. *PLoS One* 2010, 5, No. e10830.
- (39). Bondy B; Hofmann M; Muller-Spahn F; Witzko M; Hock C Reduced Beta-Amyloid Response in Lymphocytes of Patients with Alzheimer's Disease. *Pharmacopsychiatry* 1995, 28, 143–146. [PubMed: 7491368]
- (40). Monsonego A; Zota V; Karni A; Krieger JI; Bar-Or A; Bitan G; Budson AE; Sperling R; Selkoe DJ; Weiner HL Increased T Cell Reactivity to Amyloid Beta Protein in Older Humans and Patients with Alzheimer Disease. *J. Clin. Invest* 2003, 112, 415–422. [PubMed: 12897209]
- (41). Panossian LA; Porter VR; Valenzuela HF; Zhu X; Reback E; Masterman D; Cummings JL; Effros RB Telomere Shortening in T Cells Correlates with Alzheimer's Disease Status. *Neurobiol. Aging* 2003, 24, 77–84. [PubMed: 12493553]
- (42). Agrawal S; Abud EM; Snigdha S; Agrawal A IgM Response against Amyloid-Beta in Aging: a Potential Peripheral Protective Mechanism. *Alzheimer's Res. Ther* 2018, 10, 81. [PubMed: 30115117]
- (43). Jaremo P; Milovanovic M; Buller C; Nilsson S; Winblad B Alzheimer's Disease and Granulocyte Density Diversity. *Eur. J. Clin. Invest* 2013, 43, 545–548. [PubMed: 23551244]
- (44). Sollvander S; Ekholm-Pettersson F; Brundin RM; Westman G; Kilander L; Paulie S; Lannfelt L; Sehlin D Increased Number of Plasma B Cells Producing Autoantibodies Against A $\beta$ 42 Protofibrils in Alzheimer's Disease. *J. Alzheimer's Dis* 2015, 48, 63–72. [PubMed: 26401929]
- (45). Cao W; Zheng H Peripheral Immune System in Aging and Alzheimer's Disease. *Mol. Neurodegener* 2018, 13, 51. [PubMed: 30285785]
- (46). Zheng C; Zhou XW; Wang JZ The Dual Roles of Cytokines in Alzheimer's Disease: Update on Interleukins, TNF- $\alpha$ , TGF- $\beta$  and IFN- $\gamma$ . *Transl. Neurodegener* 2016, 5, 7. [PubMed: 27054030]
- (47). Lexa KW; Dolgih E; Jacobson MP A Structure-based Model for Predicting Serum Albumin Binding. *PLoS One* 2014, 9, No. e93323.
- (48). Mannini B; Mulvihill E; Sgromo C; Cascella R; Khodarahmi R; Ramazzotti M; Dobson CM; Cecchi C; Chiti F Toxicity of Protein Oligomers is Rationalized by A Function Combining Size and Surface Hydrophobicity. *ACS Chem. Biol* 2014, 9, 2309–2317. [PubMed: 25079908]
- (49). Campioni S; Mannini B; Zampagni M; Pensalfini A; Parrini C; Evangelisti E; Relini A; Stefani M; Dobson CM; Cecchi C; Chiti F A Causative Link between the Structure of Aberrant Protein Oligomers and Their Toxicity. *Nat. Chem. Biol* 2010, 6, 140–147. [PubMed: 20081829]
- (50). Deng ZJ; Liang M; Monteiro M; Toth I; Minchin RF Nanoparticle-induced Unfolding of Fibrinogen Promotes Mac-1 Receptor Activation and Inflammation. *Nat. Nanotechnol* 2011, 6, 39–44. [PubMed: 21170037]

- (51). Hardy J; Selkoe DJ The Amyloid Hypothesis of Alzheimer's Disease: Progress and Problems on the Road to Therapeutics. *Science* 2002, 297, 353–356. [PubMed: 12130773]
- (52). Kaye R; Head E; Thompson JL; McIntire TM; Milton SC; Cotman CW; Glabe CG Common Structure of Soluble Amyloid Oligomers Implies Common Mechanism of Pathogenesis. *Science* 2003, 300, 486–489. [PubMed: 12702875]
- (53). Benilova I; Karran E; De Strooper B The Toxic A $\beta$  Oligomer and Alzheimer's Disease: An Emperor in Need of Clothes. *Nat. Neurosci* 2012, 15, 349–357. [PubMed: 22286176]
- (54). Krotee P; Rodriguez JA; Sawaya MR; Cascio D; Reyes FE; Shi D; Hattne J; Nannenga BL; Oskarsson ME; Philipp S; Griner S; Jiang L; Glabe CG; Westmark GT; Gonen T; Eisenberg DS Atomic Structures of Fibrillar Segments of hIAPP Suggest Tightly Mated  $\beta$ -sheets are Important for Cytotoxicity. *eLife* 2017, 6, No. e19273.



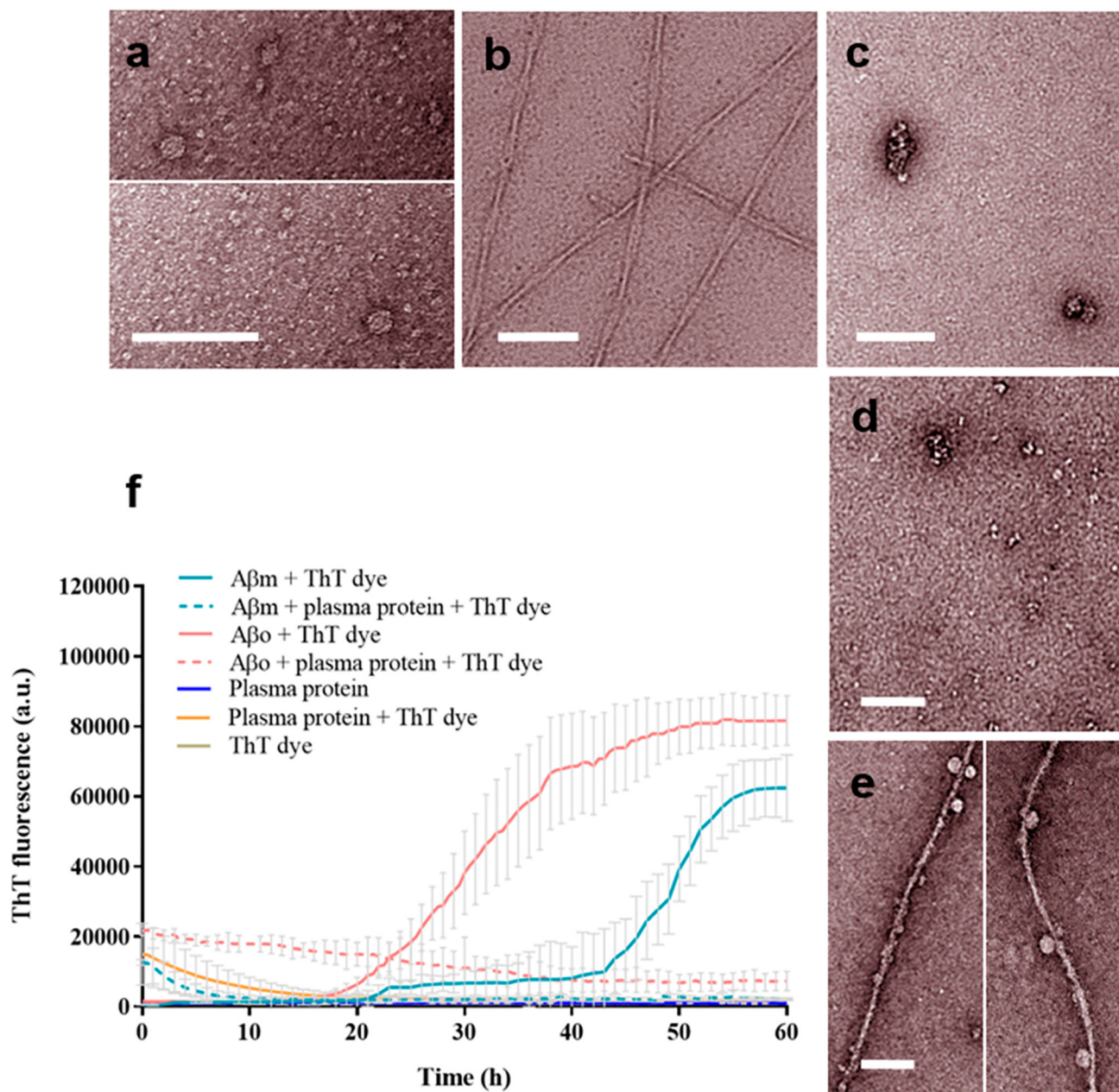


**Figure 1.**

TEM imaging and ThT kinetic assay of  $A\beta$  fibrillization. TEM images show the following structures: (a)  $A\beta_o$ , (b)  $A\beta_f$ , (c) plasma proteins, (d)  $A\beta_o$  with plasma proteins, and (e)  $A\beta_f$  with plasma proteins. The experiments were performed in triplicate. The error bars indicate the standard deviations of averaged data sets.  $A\beta$  concentration:  $50 \mu\text{M}$  (ThT assay,  $37^\circ\text{C}$ ) and  $20 \mu\text{M}$  (TEM, at room temperature). Scale bars: 100 nm. (f) ThT kinetic assay of  $A\beta_m$  and  $A\beta_o$  fibrillization with and without plasma proteins.



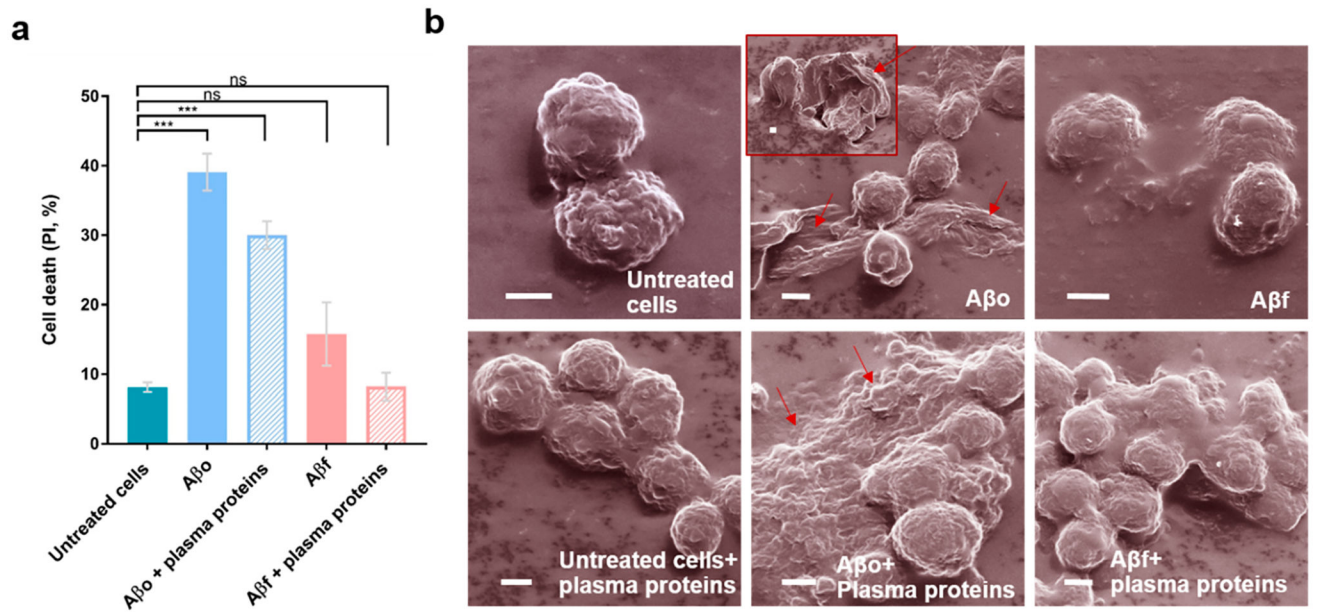


**Figure 2.**

Viability and morphology of neuronal cells exposed to the A $\beta$  species with or without plasma proteins. (a) SY5Y cell toxicities exposed to A $\beta$ o and A $\beta$ f. PI: propidium iodide. (b) Helium ion microscopy indicates the toxicity of A $\beta$  species with and without plasma proteins. Arrows indicate the deformation of cell membranes induced by A $\beta$ o. Cells were treated with the A $\beta$  species for 2 h, with or without plasma proteins. The experiment was performed in triplicate, and error bars indicate standard deviations (ns,  $P > 0.05$ ; and \*\*\*,  $P < 0.001$ ). A $\beta$  concentration: 20  $\mu$ M. Scale bars: 2  $\mu$ m.

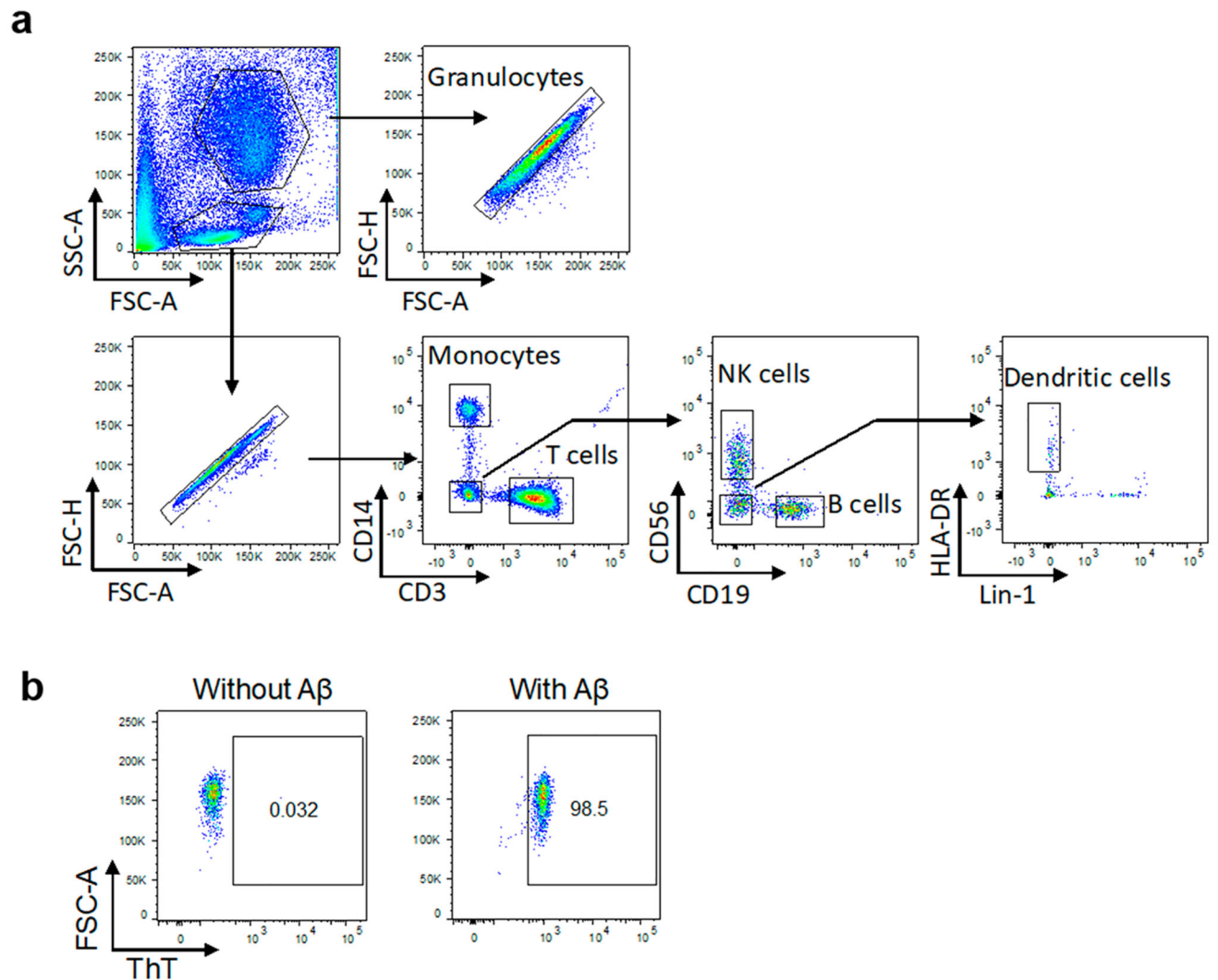


**Figure 3.**

Gating strategy used to determine white blood cell populations and amyloid association.

(a) Representative gating strategy used to determine white blood cell populations. Forward scatter area (FSC-A) and side scatter area (SSC-A) were first analyzed to locate white blood cells. Doublets were excluded based on the FSC-A vs FSC-H of single cells gated. The following cell types were identified using sequential gating based on expression of surface markers or light scatter: high SSC-A granulocytes; CD3+ T cells; CD14+ monocytes; CD56+ NK cells; CD19+ B cells; and Lin1-veHLA-DR+ dendritic cells. (b) Cell association with ThT-labeled A $\beta$  was then measured, and an example of the gating is shown for the monocyte population. Further examples can be found in the Supporting Information, Figure S3.

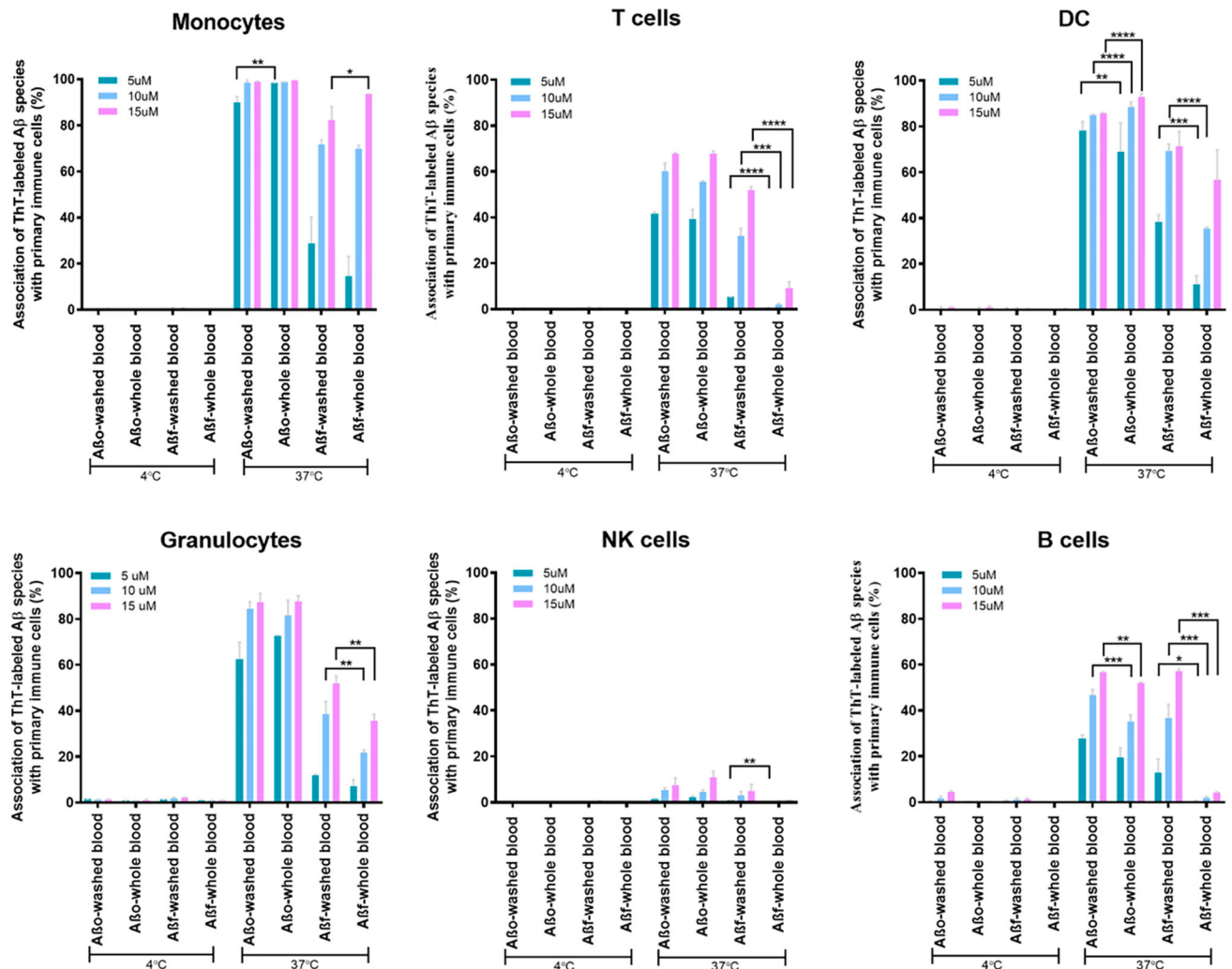


**Figure 4.**

Association of the Aβ species with immune cells. The graphs show the association of immune cells as monocytes, T cells, dendritic cells, granulocytes, NK cells, and B cells with ThT-labeled Aβo and Aβf in 3 different concentration of 5, 10, and 15 μM. The treatments with Aβo and Aβf were applied at 4 and 37 °C in whole blood (with plasma proteins) and washed blood (plasma proteins removed). Association of Aβ with cell membranes was significantly lower in whole blood than washed blood. The assay was performed in triplicate. The error bars show standard deviations (\*, *P* < 0.05; \*\*, *P* < 0.01; \*\*\*, *P* < 0.001; and \*\*\*\*, *P* < 0.0001).

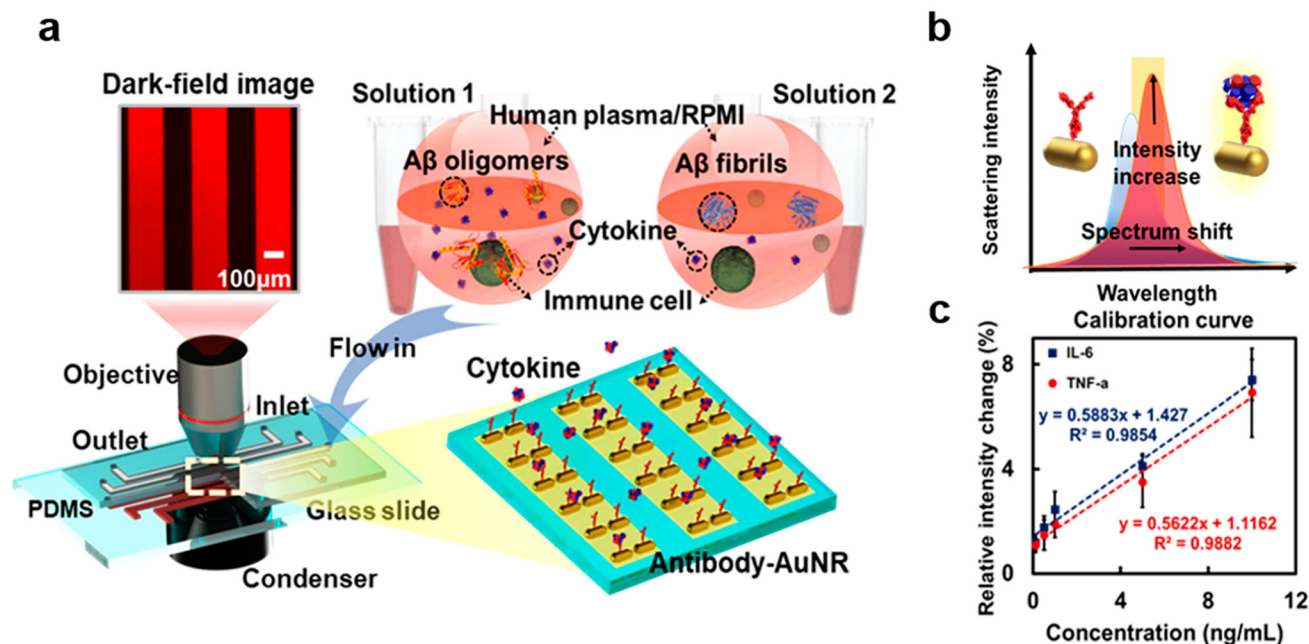


**Figure 5.** Schematics of the LSPR immunoassay. (a) LSPR immunoassay on A $\beta$ <sub>o</sub>- and A $\beta$ <sub>f</sub>-induced immune responses. Human immune cells (T cells, B cells, or THP-1 cells) were incubated with A $\beta$ <sub>o</sub> and A $\beta$ <sub>f</sub> in human plasma or RPMI medium, respectively. The cellular responses were compared by detecting secreted concentrations of TNF and IL-6 in the medium using LSPR microfluidic chips in dark field. (b) Cytokine binding with AuNR–antibody conjugates altered the local refractive index and scattering cross section of the nanostructure, giving rise to a red shift in the SRP peak coupled with an elevated scattering intensity. The cytokines secreted were determined by changes to the scattering light intensity using an EMCCD. (c) Calibrations of cytokines TNF and IL-6 showing the relative intensity changes of the LSPR barcode with varied cytokine concentrations. The trendline equations and  $R^2$  values are indicated. AuNR: gold nanorod.

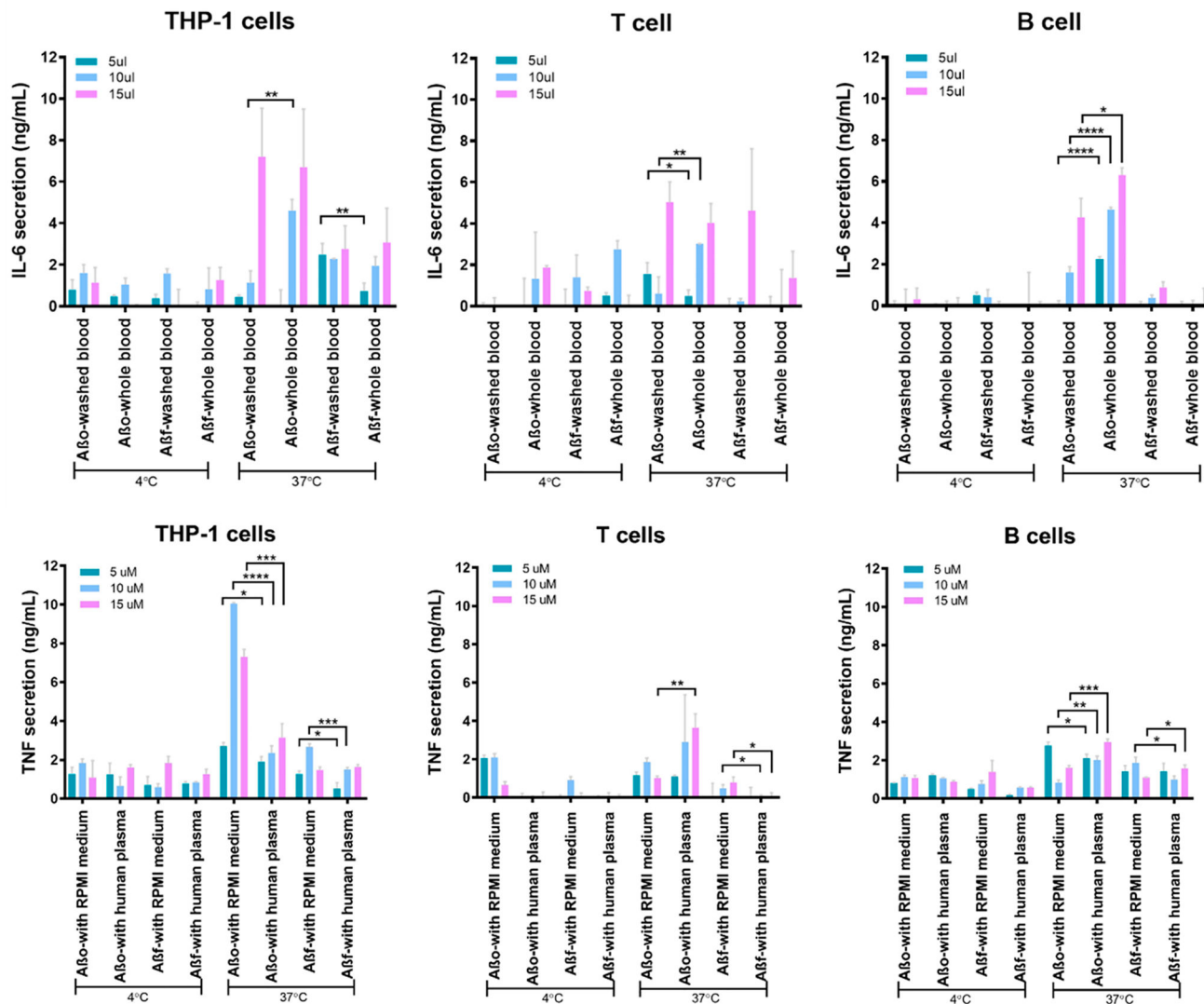


**Figure 6.** Aβ-induced immune responses of human immune cells. Cytokine secretion profiles for THP-1 cells, T cells, and B cells incubated with Aβ<sub>o</sub> and Aβ<sub>f</sub> in human plasma or RPMI-1640 medium. The assay was performed in triplicate. The error bars indicate standard deviations (\*, *P* < 0.05; \*\*, *P* < 0.01; \*\*\*, *P* < 0.001; and \*\*\*\*, *P* < 0.0001).